Title
Thermal and photochemical reactions of NO2 on chromium(iii) oxide surfaces at atmospheric pressure

Journal
Physical Chemistry Chemical Physics, 14(45)

ISSN
1463-9076 1463-9084

Authors
Nishino, Noriko
Finlayson-Pitts, Barbara J

Publication Date
2012

DOI
10.1039/c2cp42292a

Peer reviewed

PCCP

Cite this: *Phys. Chem. Chem. Phys.*, 2012, **14**, 15840–15848

www.rsc.org/pccp

PAPER

Thermal and photochemical reactions of NO_2 on chromium(III) oxide surfaces at atmospheric pressure

Noriko Nishino and Barbara J. Finlayson-Pitts*

Received 5th July 2012, Accepted 11th October 2012
DOI: 10.1039/c2cp42292a

While many studies of heterogeneous chemistry on Cr_2O_3 surfaces have focused on its catalytic activity, less is known about chemistry on this surface under atmospheric conditions. We report here studies of the thermal and photochemical reactions of NO_2 on Cr_2O_3 at one atm in air. In order to follow surface species, the interaction of 16–120 ppm NO_2 with a 15 nm Cr_2O_3 thin film deposited on a germanium crystal was monitored in a flow system using attenuated total reflectance (ATR) coupled to a Fourier transform infrared (FTIR) spectrometer. Gas phase products were monitored in the effluent of an ~285 ppm NO_2–air mixture that had passed over Cr_2O_3 powder in a flow system. A chemiluminescence NO_y analyzer, a photometric O_3 analyzer and a long-path FTIR spectrometer were used to probe the gaseous products. In the absence of added water vapor, NO_2 formed nitrate (NO_3^-) ions coordinated to Cr^{3+}. These surface coordinated NO_3^- were reversibly solvated by water under humid conditions. In both dry and humid cases, nitrate ions decreased during irradiation of the surface at 302 nm, and NO and NO_2 were generated in the gas phase. Under dry conditions, NO was the major gaseous product while NO_2 was the dominant species in the presence of water vapor. Heating of the surface after exposure to NO_2 led to the generation of both NO_2 and NO under dry conditions, but only NO_2 in the presence of water vapor. Elemental chromium incorporated into metal alloys such as stainless steel is readily oxidized in contact with ambient air, forming a chromium-rich metal oxide surface layer. The results of these studies suggest that active photo- and thermal chemistry will occur when boundary layer materials containing chromium(III) or chromium oxide such as stainless steel, roofs, automobile bumpers *etc.* are exposed to NO_2 under tropospheric conditions.

Introduction

Chromium(III) oxide (Cr_2O_3) is the most stable oxide form of chromium under atmospheric conditions and is widely used as protective and decorative coatings on various surfaces such as motor vehicle parts, appliances and hardware.[1] It possesses such advantageous properties as inertness, hardness, and resistance to corrosion and wear, as well as optical properties that give it a shiny green-colored tint.[1–6] Chromium oxide is added to paints and roofing materials to provide a green color.[4] Coatings of Cr_2O_3 thin films are also used as selective solar collectors[7] as well as for electrochromic coatings[8] and lithography masks.[9] Elemental chromium is added to metal alloys (*i.e.*, stainless steels) to provide corrosion resistance since it is selectively oxidized to form a chromium-rich oxide thin film on the surface that enhances the passivity.[1,10–13]

Many studies of heterogeneous chemistry on Cr_2O_3 surfaces have focused on its catalytic activity. Like other metal oxides (*e.g.*, V_2O_5), bulk or supported Cr_2O_3 can be used in the catalytic reduction of NO with NH_3, CO and H_2 for controlling NO_x emissions from vehicles and power plants.[14–17] Hydrogenation and dehydrogenation of alkenes and alkanes, respectively, are also known catalytic reactions on Cr_2O_3.[18] However, these heterogeneous catalyses require different pressures and temperatures than those encountered in the atmosphere, and little attention has been paid to chemistry on Cr_2O_3 surfaces under atmospherically relevant conditions.

Heterogeneous atmospheric reactions of trace gases are known to occur on surfaces in the boundary layer such as buildings, roads, vegetation and airborne particles. This can significantly impact the chemical composition of both surfaces and the gas phase.[19–21] For example, mineral dust particles contain various oxides such as SiO_2, Al_2O_3 and Fe_2O_3, and the interactions of NO_2 and HNO_3 with these surfaces lead to the formation of various nitrogen containing surface species including nitrite (NO_2^-) and nitrate (NO_3^-) ions.[22–28] Adsorbed water on oxide surfaces often has a significant effect on these heterogeneous reactions.[21–23,26,27,29,30] Enhanced surface uptake of NO_2 and HNO_3 has been reported on hydrated surfaces or in the presence of water vapor compared to dehydrated surfaces.[31,32]

Department of Chemistry, University of California, Irvine, California 92697-2025, USA. E-mail: bjfinlay@uci.edu; Fax: +1 949-824-2420; Tel: +1 949-824-7670

Photo-induced reactions on oxide surfaces have also been studied, including the direct photolysis of adsorbed species such as NO_2^- and NO_3^- on Al_2O_3 surfaces.[33,34] Photocatalytic reactions of oxide surfaces such as TiO_2 which form electron–hole pairs upon light absorption have been of considerable interest because of environmental and energy applications, including self-cleaning coatings and electrolysis of water into H_2 and O_2.[35–40] Several studies have reported photo-induced reduction of NO_2 to NO and/or HONO on TiO_2.[41–45] Recently, reduction of NO_2 to NO and HONO was observed on a stainless steel chamber surface in the dark, and this process was enhanced in the presence of light.[46] This suggests that the components of stainless steel surfaces such as Cr_2O_3 may also exhibit interesting photochemistry.

We report here studies of the thermal and photochemical reactions of NO_2 on Cr_2O_3 surfaces. The surface species formed from the interaction of NO_2 with a Cr_2O_3 thin film and the effects of water vapor were studied using attenuated total reflectance (ATR) coupled to a Fourier transform infrared (FTIR) spectrometer. In addition, a quartz flow tube containing Cr_2O_3 powder was used to measure the gas-phase products formed in the reactions. We show that adsorbed NO_2 reacts with the Cr_2O_3 surface to form nitrate ions which are reversibly solvated by water. The presence of water vapor is shown to alter the mechanisms and hence distribution of gas-phase products formed from the subsequent thermal and photochemical reactions of surface species.

Experimental

ATR-FTIR measurements of surface species

Surface species adsorbed and formed on a Cr_2O_3 surface were monitored using ATR coupled with an FTIR spectrometer (Mattson Galaxy 5020, now Thermo Electron Corp., Madison, WI). An ATR crystal (germanium, 8 cm × 1 cm × 0.4 cm, Pike Technologies, Madison, WI) was placed on a horizontal ATR holder (Pike Technologies, Madison, WI) within the FTIR optical path, where the incoming infrared (IR) beam hits the crystal at 45° angle of incidence and undergoes 10 total internal reflections along the crystal. The evanescent wave penetrates into the medium in contact with the crystal, allowing detection of surface species that absorb IR. A thin (15 nm) film of Cr_2O_3 (99.995% Strem Chemicals, Inc., Newburyport, MA) was deposited on the top surface of the ATR crystal by electron-beam evaporation. The same deposition procedure was performed on a silicon wafer to examine the uniformity of the coating using scanning electron microscopy (SEM) (Zeiss EVO® LS15). The SEM image of the coating appeared to be evenly distributed. The calculated depth of penetration[47] of the evanescent wave was 0.6–3.0 μm over the range from 4000–800 cm^{-1}, allowing for surface species above the Cr_2O_3 thin film to be interrogated.

The Cr_2O_3 film coated ATR crystal was enclosed in a 15 cm^3 volume custom reaction cell (see Fig. 1).[48] The interior walls of the cell were coated with halocarbon wax (Halocarbon Products Corporation, River Edge, NJ). The cell had inlet and outlet ports on the sides to flow desired concentrations of gases over the crystal at a total flow rate of 70 cm^3 min^{-1}. The topside of the reaction cell had a quartz window to permit irradiation of the surface. Irradiation was performed using a Double Bore® mercury pen-ray lamp whose main emission is a broad band centered at 302 nm (Jelight Company, Inc., Irvine CA) (Fig. 1). In addition, mercury lines[49] at 254, 366, 405 and 436 nm can be seen. For nitrate ion photolysis in aqueous solution, the 254 nm radiation will excite the $\pi \rightarrow \pi^*$ transition while the 302 nm excites the $n \rightarrow \pi^*$ transition.[50] Taking into account the absorption cross sections, quantum yields and relative lamp intensities in these two regions, 64% of the photolysis is estimated to occur *via* the $n \rightarrow \pi^*$ transition around 302 nm. All experiments were conducted at atmospheric pressure (760 Torr) and room temperature (295 ± 2 K), except for thermal desorption experiments, which were conducted at 323 K.

Prior to the experiments, the ATR crystal was sonicated twice with purified water (Milli-Q Plus, 18.2 MΩ cm) for 15 min and then cleaned with an argon (Oxygen Services Co., UHP, >99.999%) plasma discharge at low RF for 10 min (Plasma Cleaner Sterilizer PDC-32G, Harrick Scientific Products, Inc., Ossining, New York). The crystal was then placed in the reaction cell and purged overnight with Ultrapure air (Scott-Marrin, Inc., Ultrapure Air: THC < 0.01 ppm, CO < 0.01 ppm, NO_x < 0.001 ppm, SO_2 < 0.001 ppm, Riverside, CA). This grade of air was used throughout these studies and is simply referred to as "air" in the following discussion.

The single beam ATR-IR spectra before, during, and after the reaction were collected by averaging 1024 scans at a resolution of 4 cm^{-1}. Before entering the reaction cell, the NO_2/air flow (Scott-Marrin, Inc., NO_2 in air, 282–289 ppm, Riverside, CA) was passed through a multi-channel denuder (URG-2000-30 × 242 × -3CSS, URG Corp., Chapel Hill, NC) to remove impurities (*i.e.*, HONO and HNO_3) and further diluted with air to obtain desired NO_2 concentrations. The denuder was coated with 1 wt% K_2CO_3 and 1 wt% glycerol in methanol/water (50%/50% by volume) solution and dried overnight under N_2 flow before use. For the experiments in the presence of water vapor, humidified air was generated by passing air through two bubblers containing purified water and diluted with dry air to achieve desired relative humidity (RH).

The experiments for thermal reactions were performed using a temperature-controlled cell (FT-IR TUNNEL Cell Model TNL-120H, Axiom Analytical Inc., Irvine, CA). A rod-shaped ATR crystal (Ge, 0.3 cm × 4 cm, REF LEX Analytical Corporation, Ridgewood, New Jersey) is situated in a cylindrical sample holder in such a way that gases flow around the crystal during the experiment. In order to thoroughly coat the rod surface with a thin layer of Cr_2O_3, the deposition procedure was performed by rotating the rod 120° three times. The temperature of the cell was controlled by heated water circulating through the cell jacket. The temperature was initially set at 293 K and then increased to 323 K for the thermal reaction. Thermal experiments were also conducted using the custom flow cell shown in Fig. 1 by irradiating from the top of the cell using an IR lamp (λ > 600 nm, emission spectra measured by UV-visible spectrometry, not shown) or by immersing the cell into a water bath heated at 323 K. These experiments gave similar results.

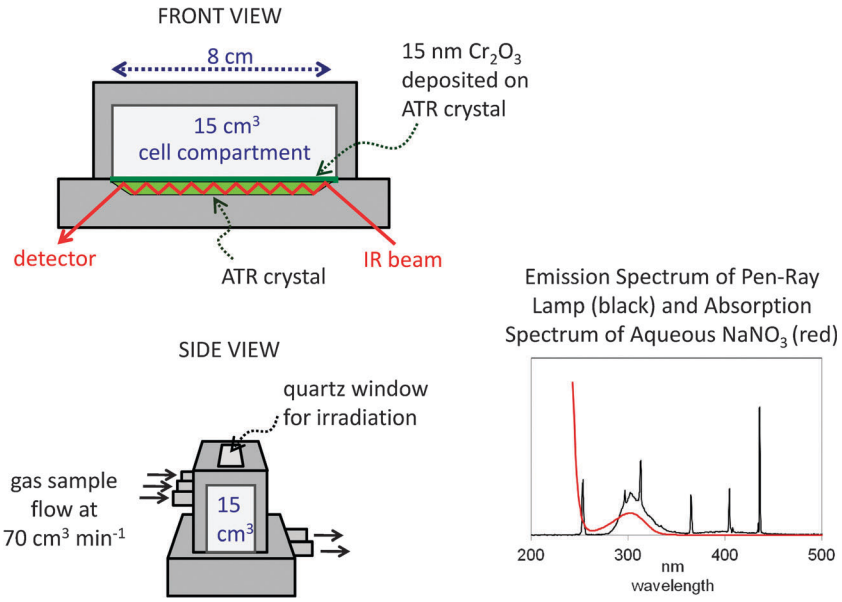

Fig. 1 Schematic diagram of custom reaction cell (front and side views) with the emission spectrum of pen-ray lamp used for irradiation (black) and the absorption spectrum of 0.4 M aqueous $NaNO_3$ (red).

For comparison to the NO_2 exposure studies, the Cr_2O_3 thin film was also exposed in separate experiments to gaseous HONO or HNO_3. Nitrous acid was generated by the reaction of gaseous HCl with solid $NaNO_2$ powder as described previously.[51,52] The concentration of HONO, 11 ppm (2.7×10^{14} molecules cm^{-3}), was measured by UV-visible spectrometry (Ocean Optics, Model HR 4000 CG-UV-NIR) using a 30 cm long quartz cell and taking the absorption cross section at 354 nm to be 2.1×10^{-19} cm^2 $molecule^{-1}$ (base 10).[53] Nitrogen dioxide was formed simultaneously in the mixture at a concentration of 9 ppm (2.1×10^{14} molecules cm^{-3}). Exposure to gaseous HNO_3 was performed by flowing air over a 1 : 3 (v/v) solution of HNO_3 (70 wt% HNO_3 99.999 + %, Sigma Aldrich) and H_2SO_4 (> 95% wt%, Fluka).

Quartz flow tube system for gas phase products

A 46 cm long custom quartz tube (i.d. 1.5 cm) was used to measure the production of gas-phase species (Fig. 2). The quartz tube was rinsed with methanol and purified water and baked at 373 K for a few hours before use. Approximately 1 g Cr_2O_3 powder (≤44 μm, 99.995% Strem Chemicals, Inc., Newburyport, MA) was distributed along the bottom of the tube, baked and irradiated for an hour to remove organic contaminants. The quartz flow tube was then flushed overnight with air at 0.5 L min^{-1}. The total flow was set at 1.6–1.8 L min^{-1} during the experiments, giving a residence time in the flow tube of 3 sec. The Cr_2O_3 powder was exposed to NO_2 (282–289 ppm) in air for 15 min and then flushed with air until the NO_y exiting the flow tube decreased below 30 ppb.

A chemiluminescence NO–NO_2–NO_y analyzer (42C model, Thermo Electron Corp., Franklin, MA) and a photometric O_3 analyzer (Model 400E, Teledyne Instruments, City of Industry, CA) were connected to the downstream of the quartz tube for the NO_y and O_3 measurements. The NO_y analyzer detects any nitrogen containing species that are reduced to NO over the catalyst, including HONO. In order to investigate the potential production of the latter species, the downstream flow was collected in a 30 L Teflon® (DuPont FEP 200A film) chamber which was then expanded into an evacuated long-path cell (1 m base path, 64 m total pathlength) mounted in the external sampling compartment of an FTIR (Research Series FTIR, now Thermo Fisher Scientific, Madison, WI). The single beam spectra were recorded at a resolution of 4 cm^{-1} with 400 scans.

For irradiation, four broad UVB lamps with the maximum intensity at 311 nm were placed parallel to the length of the quartz tube. The irradiation increased the temperature of the quartz tube up to 323 K. In order to differentiate between the thermal and photochemical changes, a thermal desorption experiment was conducted first and then the photochemical reaction was initiated. Thermal desorption experiments were conducted by heating the quartz flow tube using a heating tape. The temperature on the tube surface was measured using a thermocouple (OMEGA Engineering Inc., Stamford, CT).

The rate of photolysis of gas-phase NO_2 in the quartz tube was examined in separate experiments using UV-visible spectrometry. The quartz tube was initially filled with 96 ppm of NO_2 in N_2 (Scott-Marrin, Inc.), and the end of the tube was closed using quartz windows. The NO_2 decay was monitored as a function of time in 8 seconds. intervals using its absorbance at 400 nm during the photolysis. The photolysis rate of NO_2 was derived using rate of NO_2 decay and a series of known reactions[54] with known rate constants[55,56] that occur during NO_2 photolysis in the absence of O_2. The temperature was assumed to be constant at 308 K during the irradiation.

Results and discussion

Fig. 3a shows representative changes in the infrared absorption spectra of the surface of a 15 nm Cr_2O_3 thin film upon exposure to 120 ppm NO_2 in dry air. The absorption spectra ($A = \log S_0/S_1$) were obtained by taking the ratio of the spectrum obtained during the NO_2 exposure at various times

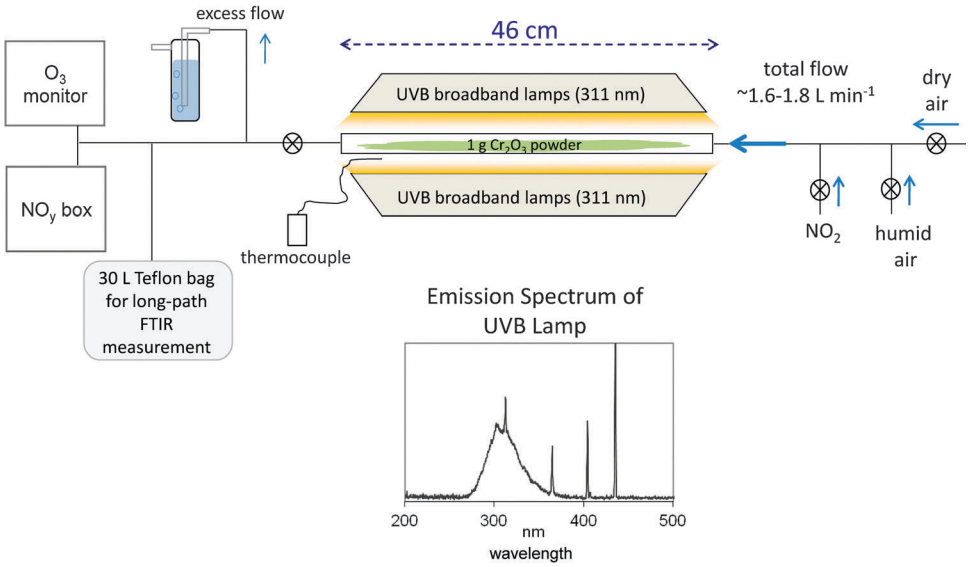

Fig. 2 Schematic diagram of quartz flow tube system with the emission spectrum of UVB lamps.

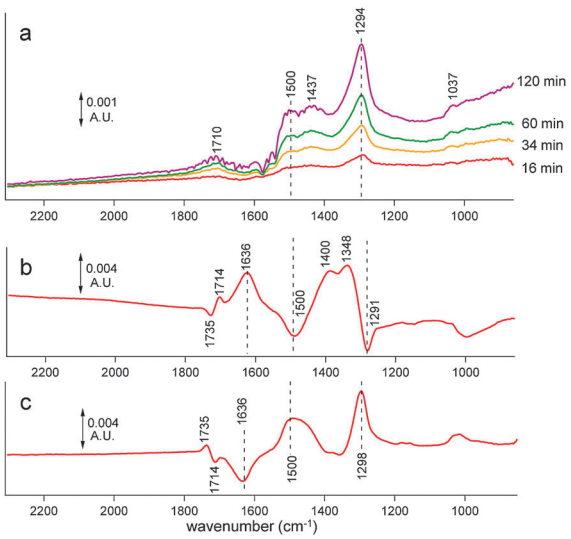

Fig. 3 Changes in absorption spectra ($A = \log S_0/S_1$) of a Ge ATR crystal coated with a 15 nm Cr_2O_3 thin film due to: (a) NO_2 (120 ppm) exposure in air for 16 min (red), 34 min (yellow), 60 min (green), and 120 min (purple), where S_0 is the spectrum taken before the NO_2 exposure and S_1 is the spectra during the exposure at various times; (b) adding humidity (70% RH) air after NO_2 exposure, where S_0 is the spectrum taken after the NO_2 exposure and S_1 is the spectrum taken when the surface is exposed to 70% RH air; (c) drying overnight after the exposure to NO_2 and then 70% RH air, where S_0 is the spectrum taken at 70% RH and S_1 is the spectrum taken when the surface is dried overnight after the exposure to NO_2 and 70% RH air.

(S_1) to the spectrum obtained immediately before the exposure (S_0). Thus, the changes shown in Fig. 3a are solely due to uptake and reaction of NO_2. Broad bands appear over the range 1280–1530 cm^{-1}, with major peaks at 1294, 1437, and 1500 cm^{-1}. Experiments conducted at a lower NO_2 concentration, 16 ppm, gave similar results. These peaks are assigned to the ν_3 stretch of NO_3^- ions based on previous studies of NO and NO_2 adsorption on amorphous Cr_2O_3 and crystalline α-Cr_2O_3.[57–60]

Although the chromium oxide thin film used here is amorphous,[61] the binding of oxides of nitrogen to chromium would be expected to be analogous to those on a crystal surface. Similar observations have been made for uptake and reaction of nitrogen oxides and HNO_3 on other metal oxides such as Al_2O_3, Fe_2O_3, and TiO_2.[22,25,26,29,32,33,62,63] The symmetric ν_1 stretch of NO_3^- is also observed at 1037 cm^{-1}.[26,32,64] An independent experiment in which Cr_2O_3 was exposed to gaseous HNO_3 showed similar peaks.

Uptake of NO_2 on surfaces such as metal oxides forms ions:[25,29,63]

$$2NO_2 \rightarrow N_2O_4 \rightarrow NO^+NO_3^- \qquad (1)$$

Nitrate ions will coordinate to Cr^{3+} ions on the surface.[25,26,29,32,57–60,62] Nitrogen dioxide can also be oxidized to NO_3^- by the oxygen on Cr_2O_3 surface.[59] Based on the frequencies of the peaks (1294 and 1500 cm^{-1}) and previous studies of nitrate ions on metal oxide surfaces,[25,32,58–60,62,63] nitrate ions are likely bound primarily in the monodentate configuration, although some contributions from the bidentate and bridging configurations cannot be excluded:[58]

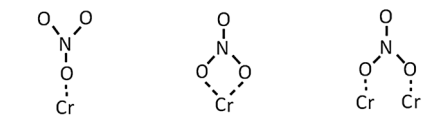

Previous studies of exposure of α-Cr_2O_3 to NO and NO_2 conducted in the absence of O_2 and water vapor under low pressures observed the formation of bidentate and bridged nitrate ions that gave rise to peaks in the ranges of 1200–1295 and 1545–1625 cm^{-1}.[57,59] The peak at 1437 cm^{-1} is attributed to partially solvated NO_3^- (see the effect of H_2O below). Although a previous study of Hadjiivanov *et al.*[59] reported nitro ($-NO_2$) species at 1348 and 1414 cm^{-1} coordinated to the surface through the nitrogen atom, these peaks were only observed after NO_3^- was established on the surface.[59]

In the present experiments, since the peak at 1437 cm^{-1} grows simultaneously with other NO_3^- peaks, we assign this to nitrate ions rather than a nitro species. A peak assignable to NO^+ was not observed here, which is not surprising since its absorption is weak.[65,66] In addition, it may be removed by reactions with other species such as trace amounts of water in the system.

Our experiments were conducted under atmospheric pressure and temperature. Thus, adsorbed O_2 and traces of water are expected on the surface, even under ostensibly dry conditions. These molecular adsorbates could interact with the surface Cr^{3+} and alter the interaction of NO_3^- with the surface.[20,67–75] For example, Hadjiivanov *et al.*[59] compared NO_2 adsorption on oxidized, reduced and hydrated surfaces of α-Cr_2O_3 that had been pretreated with O_2, H_2, and water, respectively. Both the hydrated and reduced α-Cr_2O_3 surfaces showed a higher relative abundance of bidentate NO_3^- (1294 and 1545 cm^{-1}) compared to the oxidized surfaces.[59] Grassian and co-workers[22,26] also investigated NO_2 adsorption on hydrated and non-hydrated (preheated before NO_2 adsorption) Al_2O_3 surfaces and observed broad NO_3^- bands on the hydrated surface, similar to our spectra. They interpreted the dominant peaks on the preheated non-hydrated surface as bridged and bidentate nitrate ions, while on the hydrated surface, bidentate, monodentate and partially solvated NO_3^- ions were formed.[22,26]

A small broad band is also observed at ~1710 cm^{-1}, possibly due to molecular HNO_3,[23,30–32,76,77] N_2O_4,[23,30,31,65] and/or H_3O^+.[26,78] This band was not apparent at lower NO_2 concentrations. Our HNO_3 exposure experiment showed a peak due to $\nu_2(NO_2)$ of molecularly adsorbed HNO_3 at 1700 cm^{-1}, suggesting this is responsible for at least part of the absorption in this region.

Fig. 3b shows changes in the absorption spectrum ($A = \log S_0/S_1$) when the Cr_2O_3 surface is exposed to water vapor after the NO_2 adsorption. The spectrum (S_1) was ratioed to the spectrum obtained immediately before the addition of water (S_0), so that the changes are solely due to the exposure to humid air. Peaks due to H_2O at 1636 cm^{-1} (bending mode) and 3400 cm^{-1} (OH stretching modes, not shown) as well as those due to NO_3^- complexed to H_2O at 1400 and 1348 cm^{-1} [$NO_3^-(H_2O)_n$] are observed.[22,26,32,64,76,77] Simultaneously, peaks due to $Cr^{3+}(NO_3^-)$ at 1291 and 1500 cm^{-1} decrease, indicating that the surface coordinated NO_3^- ions are converted to solvated NO_3^-. The $Cr^{3+}(NO_3^-)$ peaks are restored when the humid air is replaced by dry air (Fig. 3c), showing that the NO_3^- solvation is reversible:

$$Cr^{3+}(NO_3^-) + nH_2O \leftrightarrow NO_3^-(H_2O)_n + Cr^{3+} \quad (2)$$

A peak at 1714 cm^{-1} increases while one at 1735 cm^{-1} decreases upon the addition of water vapor. These changes reverse when the surface is dried. This suggests that the broad peak that appeared at ~1710 cm^{-1} upon NO_2 exposure (Fig. 3a) contains contributions from at least two species. In the presence of water, reaction (3) is expected to generate gaseous HONO and adsorbed HNO_3.[23,30,31]

$$NO^+NO_3^- + H_2O \leftrightarrow HNO_3 + HONO \quad (3)$$

Nitric acid forms hydrates[77] and ultimately dissociates:

$$HNO_3 + H_2O \leftrightarrow HNO_3(H_2O) \quad (4a)$$

$$HNO_3(H_2O) + H_2O \leftrightarrow HNO_3(H_2O)_2 \quad (4b)$$

$$HNO_3(H_2O)_2 + H_2O \leftrightarrow HNO_3(H_2O)_3 \quad (4c)$$

$$HNO_3(H_2O)_3 + (n-2)H_2O \leftrightarrow H_3O^+ + NO_3^-(H_2O)_n \quad (4d)$$

The fact that the 1714 cm^{-1} peak increases and the 1735 cm^{-1} decreases upon the addition of water vapor suggests that the former is due to HNO_3 and the latter to N_2O_4.

While HONO would be expected to be formed in reaction (3), gaseous HONO was not observed in the quartz tube experiments when water vapor was added after NO_2 exposure in the dark. Dissociation of HONO on the surface would also occur by reaction (5):

$$HONO \rightarrow H^+ + NO_2^- \quad (5)$$

An independent experiment was conducted to search for NO_2^- and/or adsorbed HONO on the Cr_2O_3 thin film by exposing it to gaseous HONO. No peaks due to these species were observed, but NO_3^- was formed on the surface. These observations are consistent with the oxidation of NO_2^- by NO_2 to form NO_3^-:[28,29,57,79]

$$NO_2^- + NO_2 \rightarrow NO_3^- + NO \quad (6)$$

The sequence of reactions (3), (5), and (6) would generate one NO for every 3 NO_2 molecules removed at the surface if all of the NO were released into the gas phase. In one set of experiments, NO and NO_2 concentrations were measured before and after passing over Cr_2O_3 in the quartz tube. The yield of NO was measured to be 8% of the NO_2 lost. This suggests that if reaction (6) is the sole source of NO, only part of it is released to the gas phase. This is consistent with previous reports that NO uptake onto amorphous Cr_2O_3 reacts to form nitrate ion on the surface.[58]

Changes in the absorption spectrum by heating to 323 K (spectra not shown) showed a decrease in the 1300–1500 cm^{-1} region, establishing that NO_3^- ions can be thermally removed presumably by driving reactions (4a–d) in reverse. This is consistent with a simultaneous decrease at 1703 cm^{-1}, which reflects the loss of surface HNO_3 to the gas phase. Gas-phase species formed upon heating were measured using the quartz flow tube system. Under dry conditions, there is an initial pulse of NO_2 and NO, followed by a slow decay (Fig. 4a). In the presence of water vapor, only NO_2 is generated (Fig. 4b). The small amount of NO_2 generated upon adding water vapor but before heating may be due to competitive desorption of NO_2 by water. No O_3 was formed in either experiment.

The immediate NO_2 formation upon heating under dry conditions (Fig. 4a) may partly result from the decomposition of surface-adsorbed N_2O_4 with the release of NO_2 to the gas phase:[30,53,55,56]

$$N_2O_4 \leftrightarrow 2NO_2 \quad (7)$$

Previous studies on Al_2O_3 show that molecularly adsorbed species such as N_2O_4 are weakly bound to the surface and desorb at a lower temperature than the ionic species NO_2^- and NO_3^-.[24,29] Similarly, NO has been shown in previous work to readily

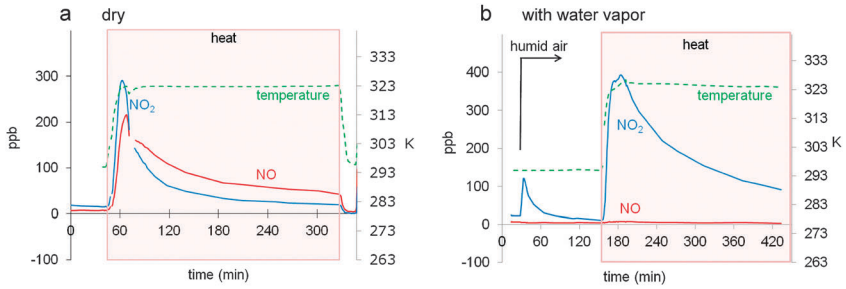

Fig. 4 Mixing ratios of NO (solid red) NO_2 (solid blue) and temperature (broken green) as a function of time when 1 g Cr_2O_3 powder previously exposed to NO_2 was heated to 323 K in a quartz flow tube in the dark under (a) dry and (b) humid conditions.

desorb from chromium oxide surfaces under dry conditions.[58,80] Nitrate ions formed on Cr_2O_3 by uptake and reaction of gaseous NO were observed to decrease upon heating to temperatures above 336 K.[58]

Nitrogen dioxide formation from the thermal decomposition of HNO_3 can be described stoichiometrically *via* reaction (8):[81,82]

$$HNO_3 \rightarrow NO_2 + 0.5H_2O + 0.25O_2 \quad (8)$$

Crowley *et al.*[82] studied the decomposition of HNO_3 on quartz surfaces and, based on the observation of NO_3 radicals, proposed mechanisms involving the autoionization of HNO_3 and the formation of N_2O_5, which then decomposes:

$$2HNO_3(l) \leftrightarrow H_2O + NO_2^+NO_3^- \leftrightarrow H_2O + N_2O_5 \quad (9)$$

$$N_2O_5 \leftrightarrow NO_2 + NO_3 \quad (10)$$

$$NO_3 \rightarrow NO + O_2 \quad (11)$$

Conversion of HNO_3 to N_2O_5 increases as temperature increases,[83] consistent with the production of NO under dry heat (Fig. 4a). However, when H_2O is added the equilibrium reaction (9) shifts to the left, quenching the formation of NO_3 and NO.[82]

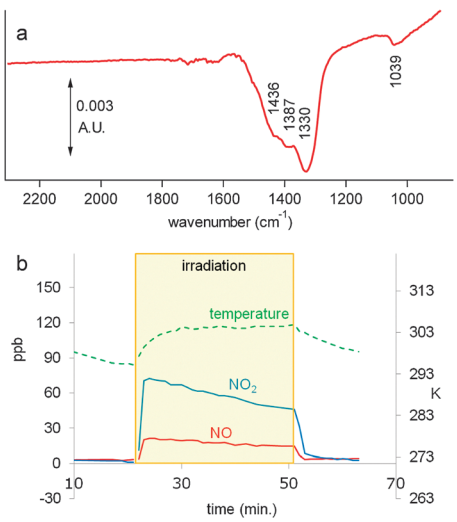

Fig. 5 (a) Changes in absorption spectrum ($A = \log S_0/S_1$) of a Ge ATR crystal coated with a 15 nm Cr_2O_3 thin film due to irradiation after NO_2 exposure under humid conditions, where S_0 is the spectrum taken after the NO_2 exposure of 120 ppm and before the irradiation and S_1 is the spectrum taken after the irradiation. (b) Mixing ratios of NO (solid red) and NO_2 (solid blue) and temperature (broken green) as a function of time when 1 g Cr_2O_3 powder previously exposed to NO_2 was irradiated in a quartz flow tube under humid conditions.

Fig. 5a shows the changes in the infrared spectrum due to irradiation in the presence of water vapor. Peaks due to solvated nitrate ions in the 1300–1500 cm^{-1} range and at 1039 cm^{-1} decrease. The major gas-phase product formed from the irradiation is NO_2, with smaller amounts of NO (Fig. 5b). The NO_2 photolysis rate in the quartz flow tube was measured as described earlier and found to be $(4.7 \pm 2.5) \times 10^{-3}$ s^{-1} (the error is 2 standard deviations). This gives a lifetime of gaseous NO_2 with respect to photolysis in this system of 4 min, much longer than the 3 s residence time in the flow tube. Thus, NO_2 loss and NO formation by gas-phase photolysis are negligible under these conditions.

The data in Fig. 5b were obtained using the NO_y chemiluminescence analyzer which measures NO specifically but reports any nitrogen oxide that is reduced to NO when the sample stream is diverted over a molybdenum catalyst as NO_2. This includes such species as HONO that are potentially produced in this system. In addition, N_2O has been reported as a product in similar systems.[33,34] To determine if nitrogen oxides other than NO and NO_2 were present, the gaseous product mixtures at 10% and 50% RH were also examined by long-path FTIR. Using available absorption cross sections,[51,84] upper limits to the yields of gas-phase HONO and N_2O relative to NO_2 were determined to be $<2\%$ and $<6\%$, respectively. This suggests either that HONO formed in reaction (3) is not released into the gas-phase or reaction (3) is not important under the conditions employed here. An X-ray photoelectron spectroscopy (XPS) study of NO_2 adsorption on Al_2O_3 also showed that the presence of molecular O_2 and adsorbed H_2O suppresses reduced nitrogen species on the surface.[27] Again, no ozone formation was observed.

It is well known that in aqueous solution NO_3^- photolyzes through two major pathways:[50,85]

$$NO_3^- + h\nu \leftrightarrow NO_2 + O^- \quad (12a)$$

$$NO_3^- + h\nu \leftrightarrow NO_2^- + O(^3P) \quad (12b)$$

The O^- ion from reaction (12a) reacts with water to form OH^- ion and OH radical, where the quantum yield for OH radical at 305 nm has been measured to be $\sim 1\%$ compared to 0.1% for $O(^3P)$ from reaction (12b).[50] Nitrite ions formed in reaction (12b) can undergo further photolysis, generating NO:[50]

$$NO_2^- + h\nu \rightarrow NO + O^- \quad (13)$$

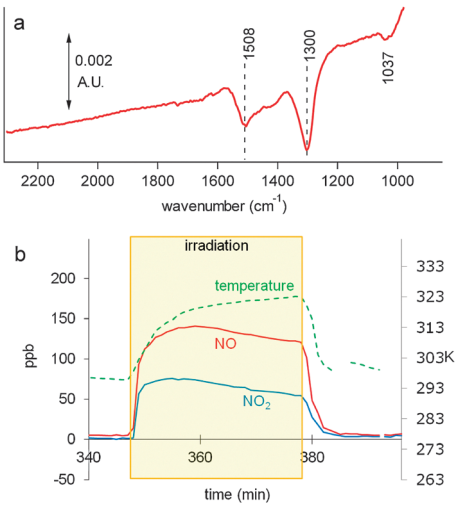

Fig. 6 (a) Changes in absorption spectrum ($A = \log S_0/S_1$) of a Ge ATR crystal coated with a 15 nm Cr_2O_3 thin film due to irradiation after NO_2 exposure under dry conditions, where S_0 is the spectrum taken after the NO_2 exposure of 120 ppm and before the irradiation and S_1 is the spectrum taken after the irradiation. (b) Mixing ratios of NO (solid red) NO_2 (solid blue) and temperature (broken green) as a function of time when 1 g Cr_2O_3 powder previously exposed to NO_2 was irradiated in a quartz flow tube under dry conditions.

Thus, the photolysis of nitrate ions on the Cr_2O_3 surface in the presence of water vapor where the infrared spectrum clearly shows the ions are solvated is qualitatively consistent with nitrate ion photochemistry in aqueous solution. As discussed below, photocatalysis involving the Cr_2O_3 may also contribute.

Under dry conditions, the $Cr^{3+}(NO_3^-)$ bands at 1508, 1300, and 1037 cm^{-1} decrease during irradiation (Fig. 6a). Both gaseous NO and NO_2 are formed (Fig. 6b), but now NO is the major product. This suggests that the mechanism of photolysis is different from that for the case where the nitrate ion is surrounded by water molecules. One possibility is that photolysis of nitrate ions coordinated to Cr^{3+} generates NO directly. On a molecular level, bidentate and bridged structures seem more likely to release NO than monodentate. A similar mechanism has been proposed by Schraml-Marth *et al.*[58]

Another possibility is that photocatalysis involving the Cr_2O_3 substrate plays a role. Photocatalysis occurs when a substrate such as TiO_2 absorbs light energy that exceeds its bandgap, resulting in formation of electron–hole pairs which participate in the reduction and oxidation of adsorbates:[35–37]

$$\text{substrate} + h\nu \rightarrow h^+ + e^- \quad (14a)$$

$$h^+ + D \rightarrow D^+ \quad (14b)$$

$$e^- + A \rightarrow A^- \quad (14c)$$

where D and A are an electron donor and acceptor, respectively. In the atmosphere, H_2O and O_2 serve as electron donors and acceptors to form the oxidants OH and O_2^-:[35,86]

$$h^+ + H_2O \leftrightarrow OH + H^+ \quad (15a)$$

$$h^+ + OH^- \leftrightarrow OH \quad (15b)$$

$$e^- + O_2 \leftrightarrow O_2^- \quad (15c)$$

The efficiency of photocatalysis depends on the lifetime of the electron–hole pairs, *i.e.*, the rate of their generation relative to the recombination rate.[35] The optical properties and the photocatalytic performance can also depend on film thickness, supporting substrate, morphology, impurities, temperature, and pretreatment of the surface.[35,36]

Photocatalysis by Cr_2O_3 is not well characterized. The reported bandgap of Cr_2O_3 varies over the range of ~2.5–4.7 eV (corresponding to ~264–497 nm) and has two possible contributions: d–d band transitions between neighboring Cr atoms (Mott–Hubbard type) and bandgap transitions between O_{2p} and Cr_{3d} bands (charge transfer type).[87,88] Irradiation of adsorbates on Cr_2O_3 can lead to either desorption or reaction, depending on the nature of the adsorbate and conditions. For example, adsorbed NO and CO undergo photo-induced desorption from Cr_2O_3 surfaces.[88–94] On the other hand, CH_3Br on α-Cr_2O_3 photodissociates at $\lambda \leq 385$ nm, while only desorption occurs at longer wavelengths.[87]

A theoretical study suggests that the hole mobility in α-Cr_2O_3 is three orders of magnitude greater than that of electrons.[95] That, combined with the presence of a negative charge on the nitrate anion, suggests a possible photocatalysis mechanism involving the formation of the nitrate radical on the surface followed by its thermal decomposition:

$$h^+ + NO_3^- \rightarrow NO_3 \quad (16)$$

$$NO_3 \rightarrow NO + O_2 \quad (17)$$

In studies of the photocatalysis of NO_2 on TiO_2, George and co-workers[45] studied the formation of gaseous products from irradiated TiO_2 that had been previously exposed to NO_2 at 30% RH and then flushed with air. They also observed both NO_2 and NO production similar to that in the present experiments (Fig. 5). They proposed that NO arose from a combination of NO_2^- photolysis, reaction (13), and reaction (16) followed by photolysis of NO_3. It should be noted that only gas-phase species were monitored in their studies and surface bound or gas-phase NO_3 radicals were not detected. In the present experiments, the light sources do not have emission lines in the region where NO_3 absorbs, so the decomposition must be thermal rather than photochemical. Thermal decomposition of NO_3 radicals in the gas-phase is well-known,[53] and a similar reaction is reasonable on surfaces.[82]

Grassian and coworkers[27] compared the uptake and reaction of NO_2 on γ-Al_2O_3 (band gap 8 eV, 150 nm) and on α-Fe_2O_3 (band gap 2 eV, 620 nm). They observed the formation of reduced nitrogen species on the α-Fe_2O_3 surface due to UV irradiation, but not on γ-Al_2O_3, consistent with photocatalytic activity of α-Fe_2O_3. They also studied the photochemistry of nitrate ions formed on Al_2O_3 by exposure to gaseous nitric acid followed by evacuation.[33,34,96,97] At the shortest irradiation times studied, NO_2 was the major gas-phase product at 20–80% RH, whereas NO dominated at RH <1%. This is similar to our observations of the interaction of NO_2 with Cr_2O_3. In short, NO_3^- photodecomposition on Cr_2O_3 surfaces may result from direct NO_3^- photolysis, photocatalysis, or a combination of the two.

This study has shown that, unlike other relatively unreactive surfaces such as SiO_2,[23,31,98] Cr_2O_3 interacts with NO_2 to form

surface-coordinated nitrate ions. These undergo both thermal and photochemical heterogeneous reactions that release NO and NO_2 back into the gas phase. This suggests that, under atmospheric conditions, Cr_2O_3 containing surfaces such as roofs, bumpers, stainless steel building materials *etc*., will take up NO_2 from the atmosphere, forming surface-bound nitrate ions. During the day, surface-bound nitrate ions undergo both thermal and photochemical heterogeneous reactions, releasing NO and NO_2 back into the gas phase.

Since a significant amount of water vapor is present in the atmosphere, the heterogeneous reactions would be similar to our results under humid conditions. To semi-quantitatively assess the potential importance of these processes, the following approach was taken. In the experiments using Cr_2O_3 powder in the flow tube, irradiation in the presence of water vapor generated 70 ppb NO_2 and 20 ppb NO (Fig. 5b), for a total concentration of 2.2×10^{12} NO_x cm^{-3}. At a typical flow of carrier gas of 1.8 L min^{-1}, this corresponds to a production rate of NO_x of 6.6×10^{13} NO_x per second. Taking a typical Cr_2O_3 particle to be spherical with a diameter of 20 μm, the one gram of powder (assuming a bulk density of 5 g cm^{-3}) used in the experiments has a total surface area of 600 cm^2. Thus the rate of NO_x production under the conditions of Fig. 5b is 1.1×10^{11} NO_x per second per cm^2 of surface, of which 22% is NO. However, this assumes that (1) the surface coverage of nitrate is the same on boundary layer surfaces as in our experimental system, and (2) the rate of photolysis of NO_3^- in the atmosphere is the same. To correct for the differences in photolysis rates, the measured rate constant for NO_2 photolysis, $k_p(NO_2) = (4.7 \pm 2.5) \times 10^{-3}$ s^{-1}, was used to calibrate the light intensity in the quartz flow tube. Thus, $k_p = \Sigma\sigma\phi F$, where σ is the NO_2 absorption cross section, ϕ is the quantum yield and F is the light intensity, all of which are wavelength dependent.[53] The relative wavelength intensities of the lamp (Fig. 2) were measured, and converted to absolute intensities using the actual measured NO_2 photolysis rate constant. This was then used to calculate the photolysis rate constant for NO_3^- in the quartz tube, assuming its absorption cross sections and photolysis quantum yields are the same as those in aqueous solution.[50,85,99,100] This gave $k_p(NO_3^-) = (1.6) \times 10^{-6}$ s^{-1} in the quartz flow tube. A similar calculation carried out using known actinic fluxes[53] at a solar zenith angle of 0° gives $k_p(NO_3^-) = (5.4) \times 10^{-7}$ s^{-1} in air. Assuming the rate of gas phase NO_x formation is proportional to the rate of photolysis of NO_3^-, the rate of NO generation from the photolysis of nitrate ions on Cr_2O_3 surfaces in the boundary layer would be 8.2×10^9 NO per second per cm^2 of surface.

This can be compared to the rate of uptake of NO_2 on such surfaces. Initial uptake coefficients for NO_2 on metal oxides[101] are typically of the order of $\gamma = 10^{-3}$–10^{-5}. However, the values decrease as the surface becomes passivated, *i.e*., covered with nitrate ions.[101] For uptake coefficients from $\gamma = 10^{-7}$–10^{-3} and an NO_2 concentration of 100 ppb, the rate of uptake of NO_2 will be in the range of 2.3×10^7 to 2.3×10^{11} molecules per second per cm^2 of surface. Thus, the emission of NO from photolysis of surface nitrate could be significant relative to the uptake of NO_2 under some conditions.

Acknowledgements

We are grateful for funding by the National Science Foundation (CHE# 0909227). We would like to thank Professor John C. Hemminger and Dr Ming Cheng for assistance with preliminary XPS studies and Dr Mo Kebaili at Integrated Nanosystems Research Facility for producing the Cr_2O_3 coating. The Carl Zeiss Center for Excellence in Electron Microscopy at University of California, Irvine, is also thanked for access to the scanning electron microscope. We are grateful to Jorg Meyer for technical assistance and to Professor James N. Pitts Jr. for helpful discussions and comments on the manuscript.

References

1 *Handbook of Materials for Product Design*, ed. C. A. Harper, Mcgraw-Hill, New York, 2001.
2 M. G. Hocking, V. Vasantasree and P. S. Sidky, *Metallic and Ceramic Coatings: Production, High Temperature Properties, and Applications*, Longman Scientific and Technical, England, 1989.
3 A. S. Kao, M. F. Doerner and V. J. Novotny, *J. Appl. Phys.*, 1989, **66**, 5315–5321.
4 C. Hornbostel, *Construction Materials: Types, Uses, and Applications*, John Wiley & Sons, Inc., New York, 1999.
5 B. Bhushan, G. S. A. M. Theunissen and X. D. Li, *Thin Solid Films*, 1997, **311**, 67–80.
6 P. Hones, M. Diserens and F. Levy, *Surf. Coat. Technol.*, 1999, **120**, 277–283.
7 M. G. Hutchins, *Surf. Technol.*, 1983, **20**, 301–320.
8 T. Seike and J. Nagai, *Sol. Energy Mater.*, 1991, **22**, 107–117.
9 F. D. Lai, C. Y. Huang, C. M. Chang, L. A. Wang and W. C. Cheng, *Microelectron. Eng.*, 2003, **67–68**, 17–23.
10 K. Budinski, *Engineering Materials: Properties and Selection*, Reston Publishing Company, Inc., Virginia, 1983.
11 C. O. A. Olsson and D. Landolt, *Electrochim. Acta*, 2003, **48**, 1093–1104.
12 I. Olefjord, B. Brox and U. Jelvestam, *J. Electrochem. Soc.*, 1985, **132**, 2854–2861.
13 L. Wegrelius, F. Falkenberg and I. Olefjord, *J. Electrochem. Soc.*, 1999, **146**, 1397–1406.
14 G. Busca, L. Lietti, G. Ramis and F. Berti, *Appl. Catal., B*, 1998, **18**, 1–36.
15 V. I. Parvulescu, P. Grange and B. Delmon, *Catal. Today*, 1998, **46**, 233–316.
16 H. Schneider, U. Scharf, A. Wokaun and A. Baiker, *J. Catal.*, 1994, **146**, 545–556.
17 B. L. Duffy, H. E. Curry-Hyde, N. W. Cant and P. F. Nelson, *J. Catal.*, 1994, **149**, 11–22.
18 B. M. Weckhuysen, I. E. Wachs and R. A. Schoonheydt, *Chem. Rev.*, 1996, **96**, 3327–3349.
19 A. R. Ravishankara, *Science*, 1997, **276**, 1058–1065.
20 H. A. Al-Abadleh and V. H. Grassian, *Surf. Sci. Rep.*, 2003, **52**, 63–161.
21 C. R. Usher, A. E. Michel and V. H. Grassian, *Chem. Rev.*, 2003, **103**, 4883–4939.
22 T. M. Miller and V. H. Grassian, *Geophys. Res. Lett.*, 1998, **25**, 3835–3838.
23 W. S. Barney and B. J. Finlayson-Pitts, *J. Phys. Chem. A*, 2000, **104**, 171–175.
24 E. Ozensoy, C. H. F. Peden and J. Szanyi, *J. Phys. Chem. B*, 2005, **109**, 15977–15984.
25 D. V. Pozdnyak and V. N. Filimono, *Adv. Mol. Relax. Processes*, 1973, **5**, 55–63.
26 J. Baltrusaitis, J. Schuttlefield, J. H. Jensen and V. H. Grassian, *Phys. Chem. Chem. Phys.*, 2007, **9**, 4970–4980.
27 J. Baltrusaitis, P. M. Jayaweera and V. H. Grassian, *Phys. Chem. Chem. Phys.*, 2009, **11**, 8295–8305.
28 J. D. Raff, J. Szanyi and B. J. Finlayson-Pitts, *Phys. Chem. Chem. Phys.*, 2011, **13**, 604–611.
29 J. Szanyi, J. H. Kwak, R. J. Chimentao and C. H. F. Peden, *J. Phys. Chem. C*, 2007, **111**, 2661–2669.

30 B. J. Finlayson-Pitts, L. M. Wingen, A. L. Sumner, D. Syomin and K. A. Ramazan, *Phys. Chem. Chem. Phys.*, 2003, **5**, 223–242.
31 A. L. Goodman, G. M. Underwood and V. H. Grassian, *J. Phys. Chem. A*, 1999, **103**, 7217–7223.
32 A. L. Goodman, E. T. Bernard and V. H. Grassian, *J. Phys. Chem. A*, 2001, **105**, 6443–6457.
33 G. Rubasinghege and V. H. Grassian, *J. Phys. Chem. A*, 2009, **113**, 7818–7825.
34 J. Schuttlefield, G. Rubasinghege, M. El-Maazawi, J. Bone and V. H. Grassian, *J. Am. Chem. Soc.*, 2008, **130**, 12210.
35 D. A. H. Hanaor and C. C. Sorrell, *J. Mater. Sci.*, 2011, **46**, 855–874.
36 M. Anpo and M. Takeuchi, *J. Catal.*, 2003, **216**, 505–516.
37 M. A. Fox and M. T. Dulay, *Chem. Rev.*, 1993, **93**, 341–357.
38 A. Fujishima, X. T. Zhang and D. A. Tryk, *Surf. Sci. Rep.*, 2008, **63**, 515–582.
39 U. Diebold, *Surf. Sci. Rep.*, 2003, **48**, 53–229.
40 A. Kudo and Y. Miseki, *Chem. Soc. Rev.*, 2009, **38**, 253–278.
41 J. S. Dalton, P. A. Janes, N. G. Jones, J. A. Nicholson, K. R. Hallam and G. C. Allen, *Environ. Pollut.*, 2002, **120**, 415–422.
42 R. J. Gustafsson, A. Orlov, P. T. Griffiths, R. A. Cox and R. M. Lambert, *Chem. Commun.*, 2006, 3936–3938.
43 M. Ndour, B. D'Anna, C. George, O. Ka, Y. Balkanski, J. Kleffmann, K. Stemmler and M. Ammann, *Geophys. Res. Lett.*, 2008, **35**.
44 S. K. Beaumont, R. J. Gustaftson and R. M. Lambert, *ChemPhysChem*, 2009, **10**, 331–333.
45 M. E. Monge, B. D'Anna and C. George, *Phys. Chem. Chem. Phys.*, 2010, **12**, 8992–8999.
46 J. Wang, J. F. Doussin, S. Perrier, E. Perraudin, Y. Katrib, E. Pangui and B. Picquet-Varrault, *Atmos. Meas. Tech.*, 2011, **4**, 2465–2494.
47 N. J. Harrick, *Internal Reflection Spectroscopy*, John Wiley & Sons, Inc., New York, 1967.
48 S. G. Moussa and B. J. Finlayson-Pitts, *Phys. Chem. Chem. Phys.*, 2010, **12**, 9419–9428.
49 J. G. Calvert and J. N. Pitts Jr., *Photochemistry*, Wiley, New York, 1966.
50 J. Mack and J. R. Bolton, *J. Photochem. Photobiol., A*, 1999, **128**, 1–13.
51 W. S. Barney, L. M. Wingen, M. J. Lakin, T. Brauers, J. Stutz and B. J. Finlayson-Pitts, *J. Phys. Chem. A*, 2000, **104**, 1692–1699.
52 L. M. Wingen, W. S. Barney, M. J. Lakin, T. Brauers and B. J. Finlayson-Pitts, *J. Phys. Chem. A*, 2000, **104**, 329–335.
53 B. J. Finlayson-Pitts and J. N. Pitts Jr., *Chemistry of the Upper and Lower Atmosphere*, Academic Press, San Diego, 2000.
54 J. R. Holmes, R. J. O'Brien, J. H. Crabtree, T. A. Hecht and J. H. Seinfeld, *Environ. Sci. Technol.*, 1973, **7**, 519–523.
55 R. Atkinson, D. L. Baulch, R. A. Cox, J. N. Crowley, R. F. Hampson, R. G. Hynes, M. E. Jenkin, M. J. Rossi and J. Troe, *Atmos. Chem. Phys.*, 2004, **4**, 1461–1738.
56 S. P. Sander, *et al.*, *Chemical Kinetics and Photochemical Data for Use in Atmospheric Studies. Evaluation Number 17.*, Jet Propulsion Laboratory, Pasadena, CA, 2011, vol. JPL Publ. No. 10-6.
57 A. A. Davydov, Y. A. Lokhov and Y. M. Shchekochikhin, *Kinet. Catal.*, 1978, **19**, 532–538.
58 M. Schraml-Marth, A. Wokaun and A. Baiker, *J. Catal.*, 1992, **138**, 306–321.
59 K. I. Hadjiivanov, D. G. Klissurski and V. P. Bushev, *J. Chem. Soc., Faraday Trans.*, 1995, **91**, 149–153.
60 K. I. Hadjiivanov, *Catal. Rev. Sci. Eng.*, 2000, **42**, 71–144.
61 M. F. Al-Kuhaili and S. M. A. Durrani, *Opt. Mater.*, 2007, **29**, 709–713.
62 A. A. Davydov, *Infrared Spectroscopy of Adsorbed Species on the Surface of Transition Metal Oxides*, John Wiley & Sons, New York, 1990.
63 D. Mei, Q. Ge, J. Szanyi and C. H. F. Peden, *J. Phys. Chem. C*, 2009, **113**, 7779–7789.
64 G. Ritzhaupt and J. P. Devlin, *J. Phys. Chem.*, 1977, **81**, 521–525.
65 J. Wang and B. E. Koel, *Surf. Sci.*, 1999, **436**, 15–28.
66 M. E. Jacox and W. E. Thompson, *J. Chem. Phys.*, 1990, **93**, 7609–7622.
67 A. Zecchina, S. Coluccia, E. Guglielm and G. Ghiotti, *J. Phys. Chem.*, 1971, **75**, 2774–2783.
68 M. Schraml-Marth, A. Wokaun, H. E. Curry-Hyde and A. Baiker, *J. Catal.*, 1992, **133**, 415–430.
69 M. A. Henderson and S. A. Chambers, *Surf. Sci.*, 2000, **449**, 135–150.
70 D. Cappus, C. Xu, D. Ehrlich, B. Dillmann, C. A. Ventrice, K. Alshamery, H. Kuhlenbeck and H. J. Freund, *Chem. Phys.*, 1993, **177**, 533–546.
71 M. A. Henderson, *Surf. Sci. Rep.*, 2002, **46**, 5–308.
72 B. Dillmann, *et al.*, *Faraday Discuss.*, 1996, **105**, 295–315.
73 P. J. M. Carrott and N. Sheppard, *J. Chem. Soc., Faraday Trans. 1*, 1983, **79**, 2425–2437.
74 B. Halpern and J. E. Germain, *J. Catal.*, 1975, **37**, 44–56.
75 A. Zecchina, S. Coluccia, L. Cerruti and E. Borello, *J. Phys. Chem*, 1971, **75**, 2783–2790.
76 P. R. McCurdy, W. P. Hess and S. S. Xantheas, *J. Phys. Chem. A*, 2002, **106**, 7628–7635.
77 K. A. Ramazan, L. M. Wingen, Y. Miller, G. M. Chaban, R. B. Gerber, S. S. Xantheas and B. J. Finlayson-Pitts, *J. Phys. Chem. A*, 2006, **110**, 6886–6897.
78 G. Ritzhaupt and J. P. Devlin, *J. Phys. Chem.*, 1991, **95**, 90–95.
79 A. L. Goodman, T. M. Miller and V. H. Grassian, *J. Vac. Sci. Technol., A*, 1998, **16**, 2585–2590.
80 H. E. Curry-Hyde, H. Musch, A. Baiker, M. Schramlmarth and A. Wokaun, *J. Catal.*, 1992, **133**, 397–414.
81 S. A. Stern, J. T. Mullhaupt and W. B. Kay, *Chem. Rev.*, 1960, **60**, 185–207.
82 J. N. Crowley, J. P. Burrows, G. K. Moortgat, G. Poulet and G. Lebras, *Int. J. Chem. Kinet.*, 1993, **25**, 795–803.
83 C. W. Tait, J. A. Happe, R. W. Sprague and H. F. Cordes, *J. Am. Chem. Soc.*, 1956, **78**, 2670–2673.
84 U.S. Environmental Protection Agency Website; http://www.epa.gov/ttn/emc/ftir/data.html Last accessed, 2012.
85 H. Herrmann, *Phys. Chem. Chem. Phys.*, 2007, **9**, 3935–3964.
86 M. R. Hoffmann, S. T. Martin, W. Y. Choi and D. W. Bahnemann, *Chem. Rev.*, 1995, **95**, 69–96.
87 M. A. Henderson, *Surf. Sci.*, 2010, **604**, 1800–1807.
88 K. Al-Shamery, *Appl. Phys. A: Mater. Sci. Process.*, 1996, **63**, 509–521.
89 S. Thiel, T. Kluner, M. Wilde, K. Al-Shamery and H. J. Freund, *Chem. Phys.*, 1998, **228**, 185–203.
90 M. Wilde, I. Beauport, K. Al-Shamery and H. J. Freund, *Surf. Sci.*, 1997, **390**, 186–193.
91 M. Wilde, O. Seiferth, K. Al-Shamery and H. J. Freund, *J. Chem. Phys.*, 1999, **111**, 1158–1168.
92 S. Borowski, T. Kluner, H. J. Freund, I. Klinkmann, K. Al-Shamery, M. Pykavy and V. Staemmler, *Appl. Phys. A: Mater. Sci. Process.*, 2004, **78**, 223–230.
93 T. Kluner, *Isr. J. Chem.*, 2005, **45**, 77–95.
94 S. Thiel, T. Kluner, D. Lemoine and H. J. Freund, *Chem. Phys.*, 2002, **282**, 361–370.
95 N. Iordanova, M. Dupuis and K. M. Rosso, *J. Chem. Phys.*, 2005, **123**, 074710.
96 H. Chen, J. G. Navea, M. A. Young and V. H. Grassian, *J. Phys. Chem. A*, 2011, **115**, 490–499.
97 G. Rubasinghege, S. Elzey, J. Baltrusaitis, P. M. Jayaweera and V. H. Grassian, *J. Phys. Chem. Lett.*, 2010, **1**, 1729–1737.
98 G. M. Underwood, C. H. Song, M. Phadnis, G. R. Carmichael and V. H. Grassian, *J. Geophys. Res., [Atmos.]*, 2001, **106**, 18055–18066.
99 P. K. Hudson, J. Schwarz, J. Baltrusaitis, E. R. Gibson and V. H. Grassian, *J. Phys. Chem. A*, 2007, **111**, 544–548.
100 N. K. Richards, L. M. Wingen, K. M. Callahan, N. Nishino, M. T. Kleinman, D. J. Tobias and B. J. Finlayson-Pitts, *J. Phys. Chem. A*, 2011, **115**, 5810–5821.
101 V. H. Grassian, *Int. Rev. Phys. Chem.*, 2001, **20**, 467–548.

